Chapter 2
Analysis of a Composite Pi/T-Joint Using an FE Model and DIC

Chris Sebastian, Mahmoodul Haq, and Eann Patterson

Abstract An analysis of composite Pi/T-joint was performed through the comparison of a finite element simulation and experimental results obtained using digital image correlation. The finite element simulation was performed in ABAQUS using a realistically modeled adhesive layer consisting of cohesive zone elements. The composite Pi/T-joints were manufactured using vacuum assisted resin transfer molding (VARTM). The resulting Pi/T-joints were loaded in out-of-plane (web pull-out) until failure, during which three-dimensional digital image correlation (3D-DIC) was used to measure the in-plane displacements and strains.

From the experiments, it was found that the average peak pull-out force was 12.56 ± 0.82 kN, which was 10 % less than that from the FE simulation at 13.77 kN. However, this does not give much information about whether the stress and strain distribution has been accurately predicted by the simulation. To better understand this, the experimental data obtained using DIC was compared to that from the FE simulation using image decomposition. The image decomposition process reduces the large, full-field data maps to a feature vector of 130 or so elements which can be compared much more easily. In this case, there was good agreement between the experiment and simulation, when taking into account the experimental uncertainty.

Keywords Composite joint • VARTM • Digital image correlation • Numerical simulation

2.1 Introduction

Composite Pi-joints are being extensively used in the marine and aerospace industries and are called T-joints, or Tee joints in some sectors. ‘T’ refers to the parts being joined while ‘Pi’ describes the shape of the preform used to form the joint. These joints are of special importance due to their complex geometry and criticality to overall structural integrity. T-joints are found at composite bulkhead-to-skin, rib-to-skin and spar-to-skin interfaces [1]. T-shaped stiffeners are extensively used in aircraft wings [1]. Additionally, the requirement for reduced structural weight and the ever-increasing demand for efficient aerospace structures has driven the development of adhesively bonded T-joints. However, these joints have been found to be sensitive to peel and, or delamination and through-the-thickness stresses. It has been reported that composite T-joints often fail near the web/skin interface [2].

Various configurations of composite T-joints have been studied extensively, mostly in the context of marine structures [3–18], including tee-joints made of sandwich panels [9–12]. The damage and failure analysis of such marine composite joints has also been studied [13–18]. A good overview on adhesively bonded composite joints is provided by Banea and Silva [19]. Moreover most of the aforementioned T-joints were manufactured by connecting the horizontal (flange) and vertical (web) laminates with a hand-layup laminate/skin (overlaminate). Similarly, literature on T-joints using a pi-preform (hence a Pi-joint) is relatively limited [20]. The use of Pi-preforms compared to hand-layup skins offers ease of manufacturing and speedy construction. Researchers from the Wright Patterson Air Force Research Laboratory (AFRL), Ohio, US, have studied adhesively bonded Pi-preform T-joints and also incorporated them in an aircraft wing and reported enhanced performance relative to a similar wing manufactured by conventional methods [2, 21, 22]. In addition, they tested the wings with T-joints

C. Sebastian (✉) • E. Patterson
School of Engineering, University of Liverpool, Liverpool L69 3GH, UK
e-mail: c.sebastian@liverpool.ac.uk

M. Haq
Composite Vehicle Research Center, Department of Civil and Environmental Engineering, Michigan State University, Lansing, MI 48910, USA

G.L. Cloud et al. (eds.), *Joining Technologies for Composites and Dissimilar Materials, Volume 10*
Conference Proceedings of the Society for Experimental Mechanics Series, DOI 10.1007/978-3-319-42426-2_2

in fatigue and found no failure in the joints [21, 22]. They reported considerable savings in manufacturing time (days instead of weeks) and up to 75 % reduction in costs. Apart from the AFRL study [2, 21, 22], the literature on pre-form Pi-joints is relatively limited. Hence, this work focuses on evaluating the pull-out performance using both structural tests to destruction and integrated experimental and simulation approach to analyzing the strain fields in structural Pi-preform composite T—joints.

In this work, the out-of-plane behavior or pull-out performance behavior of the composite Pi-joints was experimentally studied by using three-dimensional Digital Image Correlation (3D DIC). To the best of author's knowledge, the use of DIC to study the composite Pi-joints is unique and no other work has been reported, except the preliminary results reported earlier by the authors [23, 24]. The following sections provide brief details on the manufacturing process, materials used, and the experimental and numerical results.

2.2 Experimental Method

2.2.1 Manufacture of the Pi-joints

The Pi-joints of dimensions shown in Fig. 2.1 were manufactured by connecting flange and web plates with a Pi-preform and infusing the resin (adhesive) using vacuum assisted resin transfer molding (VARTM). The VARTM technique was also used to manufacture the glass fiber composite adherends (base and web plates) for the Pi-joints. The reinforcement used for the adherends was Owens Corning ShieldStrand S, S2-glass plain weave fabric with areal weight of 818 g/m^2. The base and web plates had 16 and eight layers of plain weave glass fabric respectively resulting in cured thicknesses of 9.53 mm (3/8 in.) and 4.76 mm (3/16 in.), respectively. The resin used was a two part toughened epoxy (SC-15, Applied Poleramic). The base and web plates were then connected with the Pi-preform and infused with SC-15 adhesive. The Pi-preform used was a carbon-fiber 3D woven preform (Albany Engineered Composites, Inc., Rochester, NH, USA.).

A constant adhesive bond-line thickness in Pi-joints was maintained by placing steel wires of 0.127 mm (0.005 in.) diameter in the bond-line. These spacers were placed strategically such that they did not influence the resulting performance. The tensile properties of the adhesive were obtained from experimental tests following the ASTM D638 standard. The fracture properties of the resin were obtained experimentally from Mode-I and Mode-II tests. The properties of the flange and web plates were also obtained experimentally. A summary of the material properties is provided in Table 2.1.

All bonded surfaces were grit-blasted and then cleaned with acetone. Figure 2.2 provides a step-by-step overview of the Pi-joint manufacturing process. Figure 2.2b shows the aluminum mold used to obtain the desired pi-preform dimensions. The aluminum mold has inlet and outlet pipe-fittings that attach to the vacuum pump and the resin-bath, respectively. The inlet

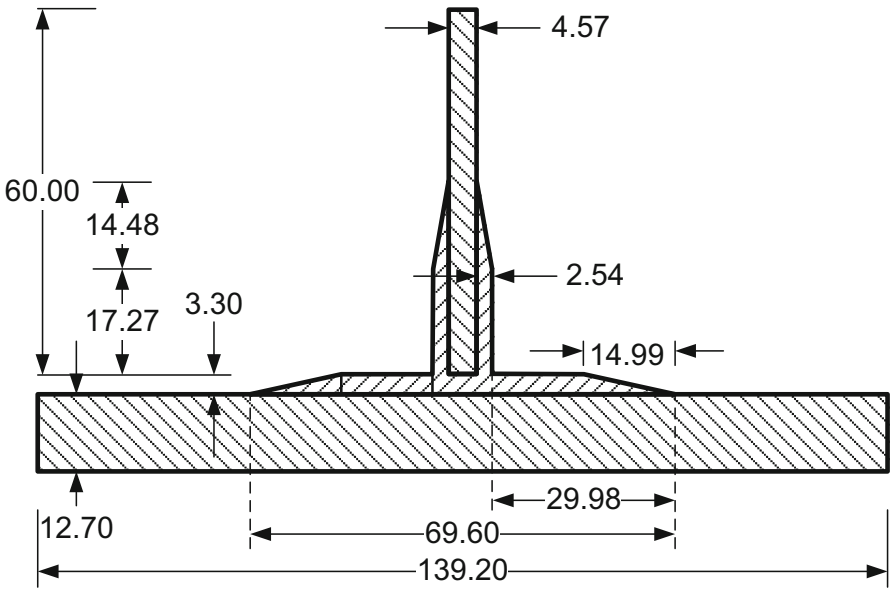

Fig. 2.1 Pi-joint dimensions (in mm) with the adhesive thickness omitted. Not to scale

Table 2.1 Material properties used in the numerical simulation

(a)	Adhesive tensile properties (experimental)	
	Modulus (GPa)	2.69 ± 0.19
	Tensile strength (MPa)	58.10 ± 3.94
	Tensile failure elongations (%)	3.45 ± 0.37
(b)	Adhesive fracture toughness [29]	
	GI_c (N/m)	0.132
	GII_c (N/m)	0.146
(c)	Plates—GFRP (experimental)	
	Web, tensile modulus (GPa)	17.25
	Base, flexural modulus (GPa)	7.00
	Poisson's ratio [5]	0.17
(d)	3D-Preform—CFRP [30]	
	Elastic, isotroPic modulus (GPa)	32.8
	Poisson's ratio	0.17

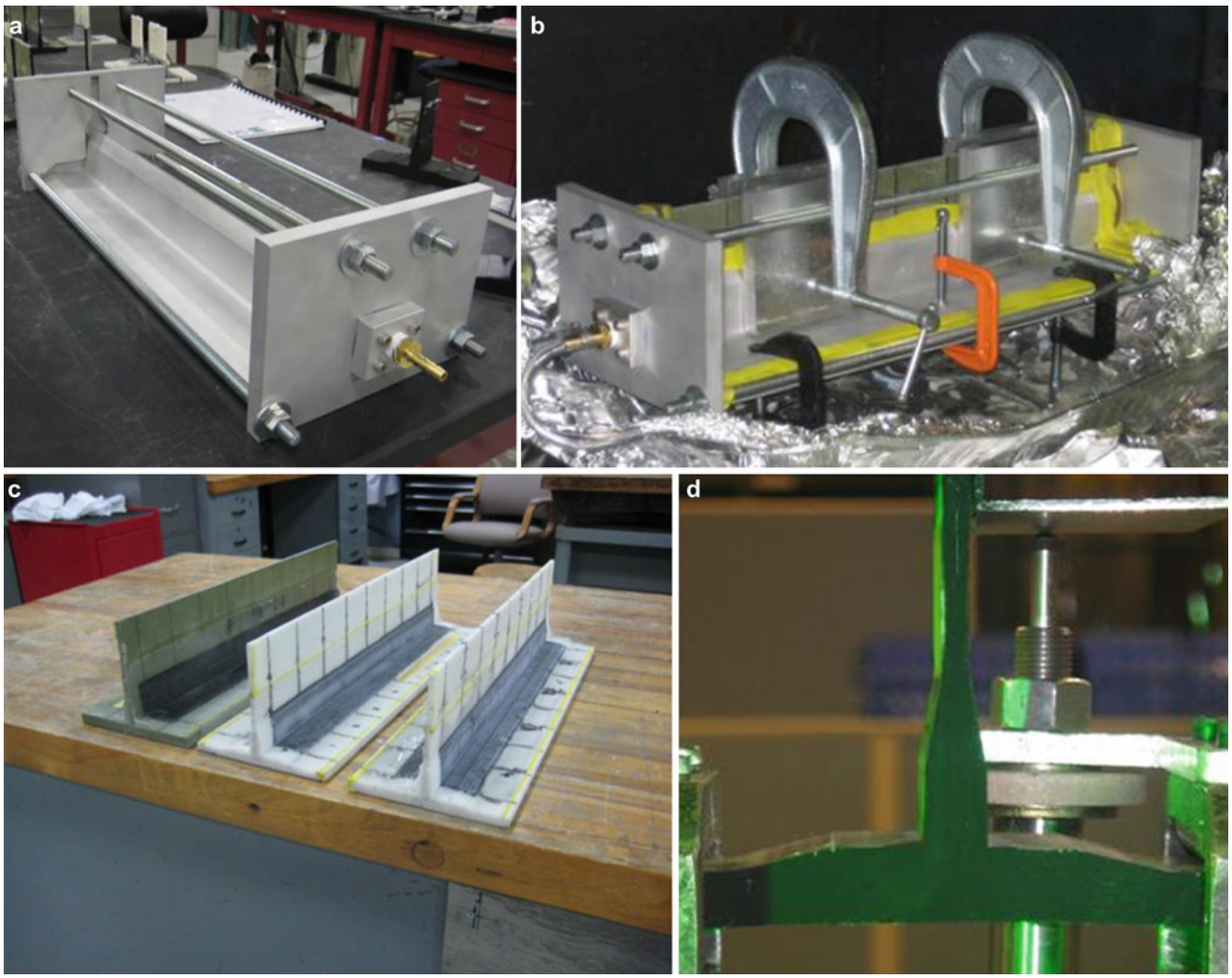

Fig. 2.2 Manufacturing of the Pi-joint using VARTM: (**a**) aluminum mold, (**b**) assembled pi-joint during VARTM, (**c**) completed pi-joints, and (**d**) a 50 mm wide section of pi-joint during a tensile pull-out test

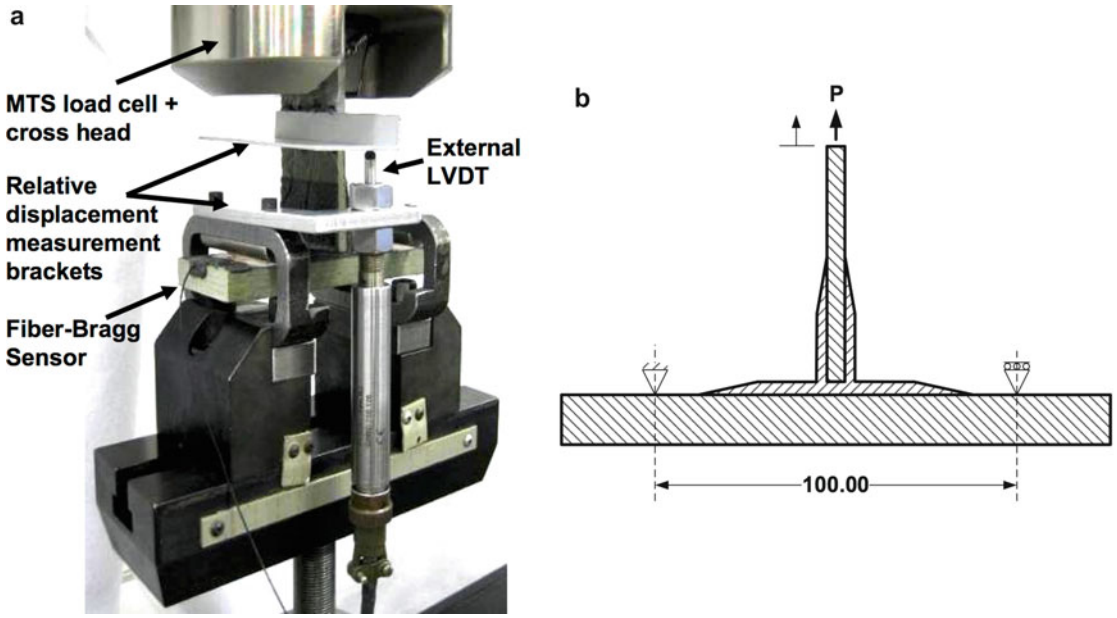

Fig. 2.3 Picture of a typical pull-out test setup (**a**); schematic of the experimental test setup (**b**)

and outlet are located just above the web-location of the Pi-preform. The permeability of the preform was found to be sufficient for successful manufacture of the Pi-joints, and hence, a distribution media was not required. The aluminum mold was fitted with end-plates and enclosed with vacuum tape prior to infusion as shown in Fig. 2.2c. The resin-infused joint was cured in a convection oven at 60 °C for 2 h and post cured at 94 °C for 4 h. The completed joints, which are shown in Fig. 2.2c, were then cut into sections of 50 mm wide using a water jet prior to being subjected to experimental testing as shown in Fig. 2.2d.

2.2.2 Pull-Out and Damage Resistance (DIC)

The out-of-plane behavior of the Pi-joints was evaluated by performing pull-out tests on the manufactured Pi-joints using a specially designed rig in a servo-hydraulic test machine, as shown in Fig. 2.3a. The specimens were tested at a loading rate of 1 mm/min until failure. The load and displacement from the test machine cross-head was recorded. Additionally, an external LVDT (linear voltage displacement transducer) was used to measure the relative displacement of the web with respect to the support.

In addition to the load and displacement values measured during the pull-out tests, a 3-D Digital Image Correlation system was employed to measure the full-field displacement and strains on the cut surface of the pi-joint. This was a commercially available DIC system (Dantec Dynamics Q-400) which consisted of a pair of cameras (AVT F-125B) along with a matched pair of lenses with a 12 mm focal length. Illumination was provided using a small panel of green LEDs. The cut surface of the Pi-joint was prepared by painting it first with a coat of matte white spray paint (Krylon matte white) and then misting with matte black (Krylon matte black) to provide the contrasting speckle pattern. Reference images for the correlation process were captured with a small pre-load applied to the joint, in order to remove any slack from the experimental setup. Images were then captured in 500 N increments up until failure of the joint occurred.

2.3 Numerical Simulations

An integrated approach to numerical simulations and experiments was taken with the intention of using simulations to facilitate the design of the experiments, sensor placement and also to support the interpretation of the experimental data, as well as creating a validated numerical model that could be used in future design work with a high-level of confidence. In this work, simulations of Pi-joint pull-out behavior were performed using a commercially-available finite element package, ABAQUS® [25].

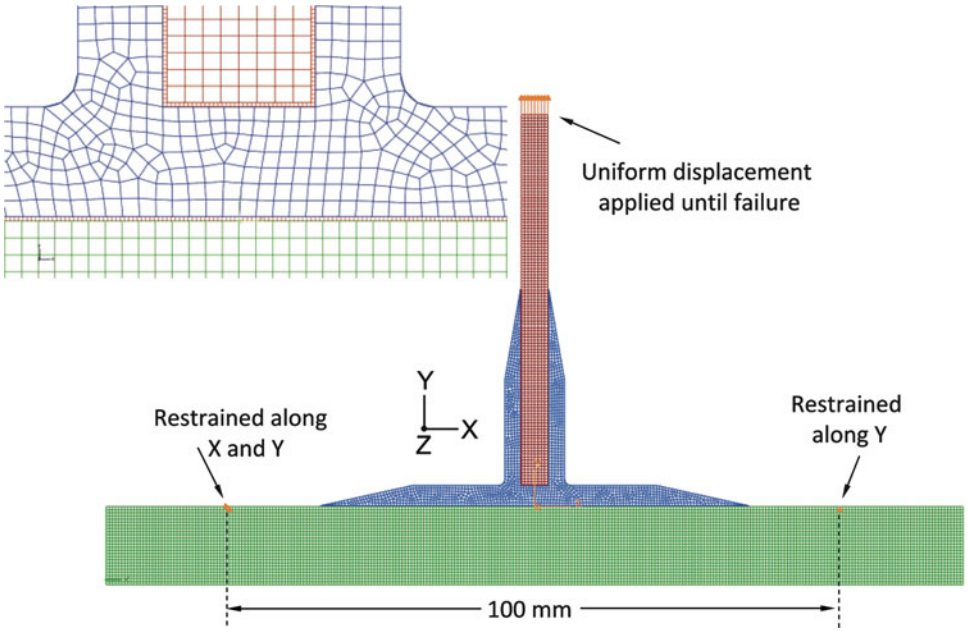

Fig. 2.4 Details of the FE model showing the boundary conditions and applied loading. The *inset* shows a more detailed view of the mesh with the quadrilateral elements and the adhesive elements

A two-dimensional plane-stress model of the Pi-joint was created in ABAQUS®. The web, flange and the pre-form were created as separate parts for ease of defining the properties and also the meshing. The adhesive was also created as a separate part but with a much finer mesh using cohesive elements. The adhesive surfaces were appropriately connected with respective surfaces of the web, flange and pre-form to assemble the model. Models that reproduced the three cases studied in the experiments were analyzed.

2.3.1 Mesh, Gap Creation and Material Models

Four-node quadrilateral plane-stress elements were used to mesh all the parts of the model in ABAQUS®. All parts were given an out-of-plane thickness of 50 mm corresponding to the width of the Pi-joint in the experiment. The flange, web and Pi-preform were modeled as linear elastic materials. An element size of 0.5 mm was used for all parts except the adhesive layers. A meshed finite element model for a Pi-joint is shown in Fig. 2.4. For adhesive layers, cohesive elements, the mesh was more refined as illustrated in the inset of Fig. 2.4. The element size of cohesive elements was equal to bond-line thickness (0.005 in., 0.127 mm), and an aspect ratio of 1 (unity) prior to load application. The adhesive was modeled in greater detail using cohesive elements and the delamination was simulated using a traction-separation material model [25]. The damage evolution was modeled in ABAQUS by defining the fracture energy as a function of the mixed modes using the analytical power law fracture criterion. The material properties used in the simulations are provided in Table 2.1.

2.3.2 Boundary Conditions and Loading

The loading pattern and boundary conditions used in the experiments were replicated in the finite element models. A schematic of the FE model is provided in Fig. 2.4. It has been reported that the number of degrees of freedom at the constraints and the angle of loading play a vital role in the accuracy of the results [6]. Kesavan et al. [6] simulated marine composite T-joints and applied the loading at an angle of 0.55° to the positive Y-axis in Fig. 2.4, to take into account manufacturing inconsistencies, and found good agreement with their experimental results. In this work, the web was assumed to be perfectly perpendicular and the angle of loading was not considered. The applied load was distributed along the top nodes in the web. The model was constrained symmetrically at two points on the flange simulating a simply-supported condition with a total span of 100 mm. The left-hand side support constraint does not permit translation in either the X- or Y-direction while the right-hand support constraint does not permit translation in the Y-direction. All simulations were performed on an eight-core 3.16 GHz machine with 64 gigabytes of RAM.

2.4 Results and Discussion

2.4.1 Experimental Pull-Out Results

Figure 2.5 provides the pull-out performance of the Pi-joints from the experiments. The general failure mode in the experiments for the Pi-joints consisted of an increasing load until failure, which led to the separation of the Pi-preform from the base. The failure was instantaneous and the direction of failure propagation could not be seen with the naked eye. A high-frame rate camera would be required to confirm the propagation path of failure. Since symmetric failure initiation was observed, the delamination propagation was also expected to be symmetric. Instead an asymmetric failure was observed. Such a discrepancy may be caused by a combination of eccentricity in load application and manufacturing flaws. The use of a brittle adhesive, like the one used in this work, makes the joint highly susceptible to manufacturing flaws and less tolerant to damage.

2.4.2 Digital Image Correlation Results

Digital Image Correlation was used to capture the displacement and strain on the cut surface of the Pi-joint as it was loaded in the tensile test. The images were processed using commercial software (Dantec Dynamics Istra 4D) to calculate the displacements and strains in the Pi-joint. A facet (or subset) size of 25 pixels was used, with an offset (or shift) of 15 pixels. The measured surface strain in the x-direction is shown in Fig. 2.7 at an applied load of 3 kN. The two red boxes indicate the areas for comparison with the FE results.

2.4.3 Numerical Simulation Results

The finite element (FE) simulations successfully modeled the complete pull-out response of the damaged and undamaged Pi-joints and the results are shown in Fig. 2.5. Figure 2.6 shows the failure mechanisms observed in the FE simulation. The initial onset of failure occurs in the web/Pi region (see inset in Fig. 2.6) and continues asymmetrically on one side of the web. This onset of failure does not reduce the load carrying capacity as the load transfer continues mostly across the other bonded

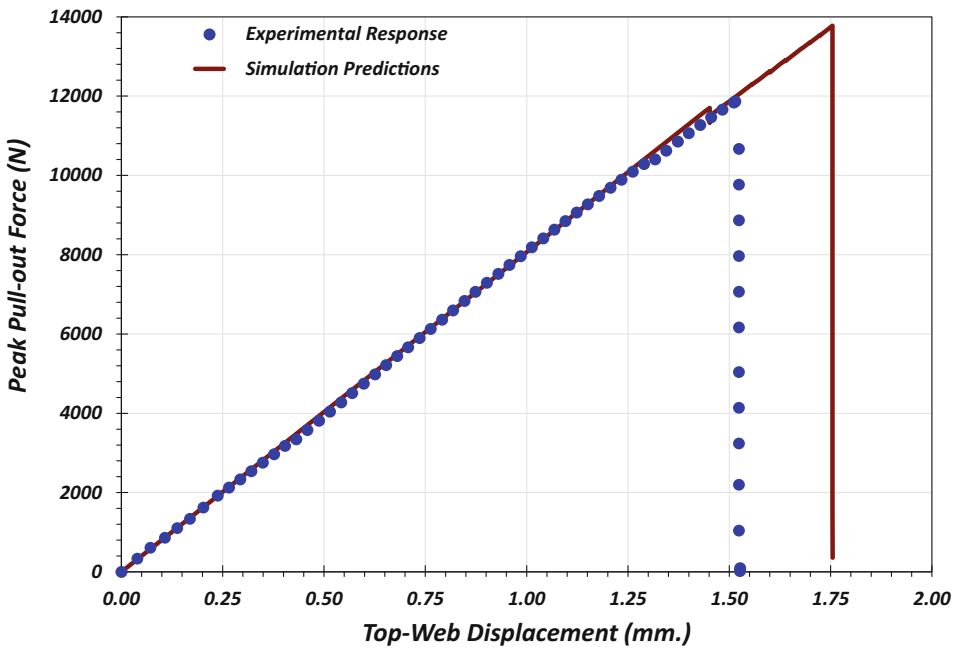

Fig. 2.5 Comparison of the complete pull-out response of the experiment and the FE simulation

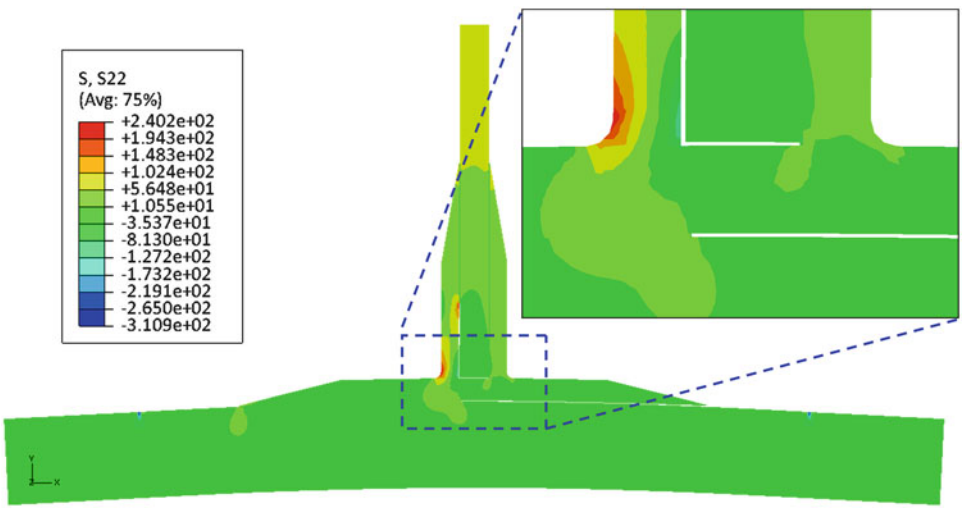

Fig. 2.6 Failure mechanism for the pi-joint in the simulation

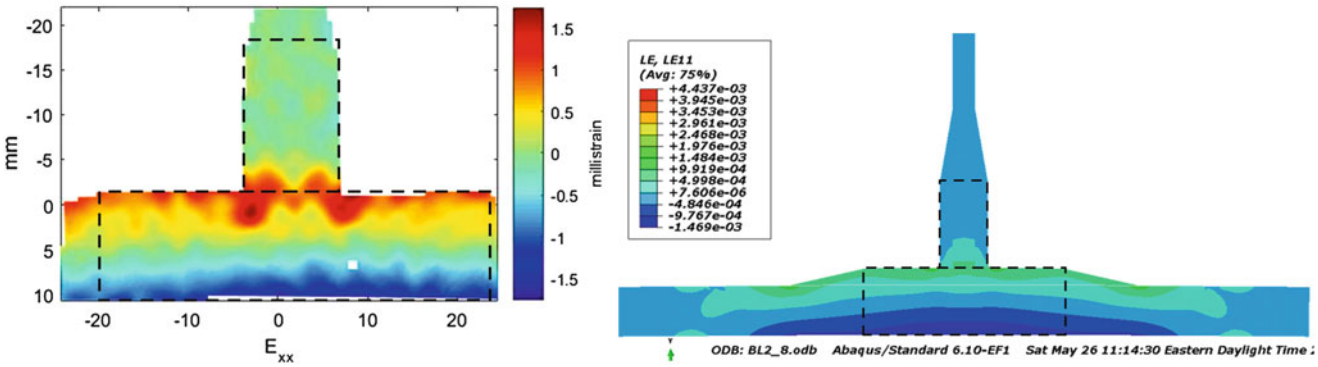

Fig. 2.7 Comparison of the principal strain from DIC (*left*) and FE (*right*). The highlighted boxes indicates where there the image decomposition comparison was performed

side of the web/Pi. As the applied load increases, the subsequent onset of failure occurs in the adhesive/bond between the preform and the base. This failure initiated from the termination of the preform with the base and continues until separation of the Pi-preform from the base.

The peak pull-out loads from the simulations agreed very well with the average experimental data as shown in Fig. 2.5. Similar load eccentricity and mis-alignment issues have been reported by Kesavan et al. [6] who applied the pull-out load at an angle of 0.55° counterclockwise to the vertical axis (web) in order to obtain better agreement between experimentation and computational results. Such modifications were not considered made in this study and all loads were applied to the web.

Additionally, the experimental data provided in Fig. 2.5 shows the standard deviation (as error bars) for each Pi-joint studied. The variation in experimental data may be due to many factors including manufacturing inconsistencies, variation in material properties of constituents, errors induced in experimental test-setup, instruments etc., Similarly, the numerical simulations assume average material properties and ideal test configurations.

2.4.4 Comparison of DIC and FE Using Image Decomposition

Although the pull-out force data matched well between the experiments and the simulation, it was desired to perform a more thorough validation of the simulation. Figure 2.7 shows the measured strain in the x-direction from the DIC experiment (left) compared to the x-strain found from the FE simulation (right). A recently published CEN document [26] recommends the use of image decomposition using Tchebichef polynomials to make quantitative comparisons of measured and predicted strain fields as part of a model validation process, This approach, which has been used previously to validate models of a

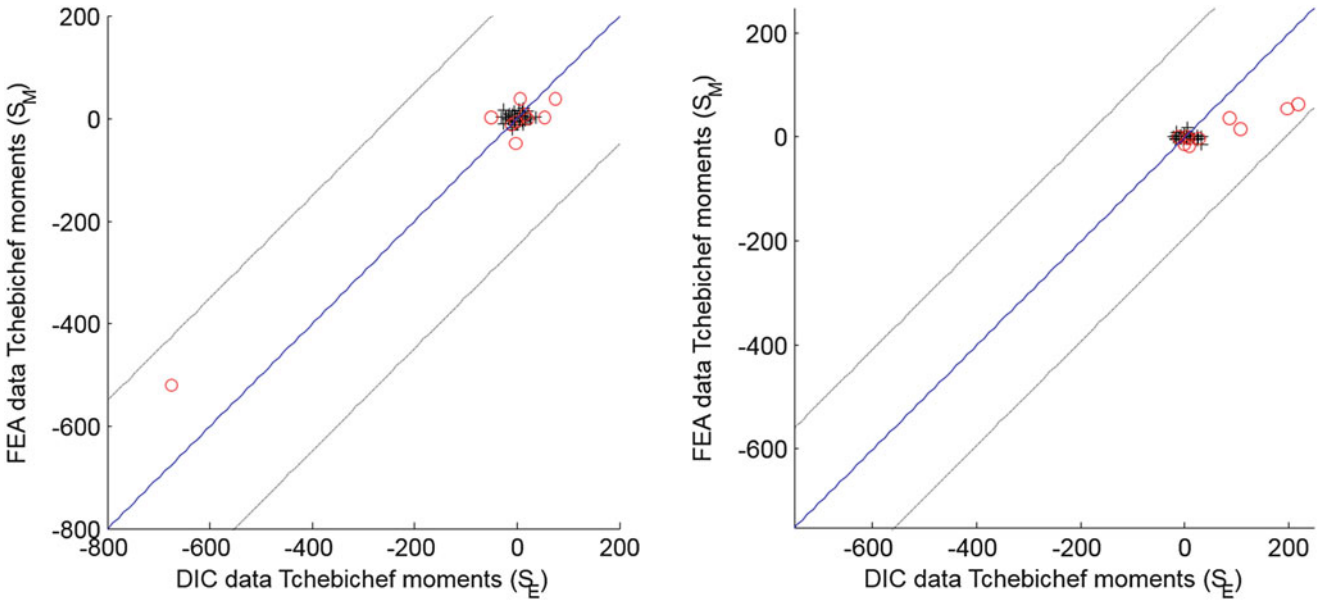

Fig. 2.8 Comparison plots of the most significant moments from the experiment and the simulation for the horizontal section (*left*) and the vertical section (*right*). If the data were in perfect agreement, all points would fall on a line with a gradient of unity (*solid line*) the dashed lines represent confidence bands equal to twice the uncertainty in the data from the experiments

vibrating plate [27] and a composite protective panel [28], was adopted here. The image decomposition using the discrete Tchebichef moments can only be performed over a rectangular domain, so the pi-joint was divided into two section for analysis. One rectangular patch was taken from the vertical section, and another from the horizontal section.

The Tchebichef polynomials were used to represent the strain component in the x-direction from both the experiment and the simulation following the procedure described in [28]. A reconstruction of the original strain image was performed from the Tchebichef coefficients to ensure that they were an accurate representation of the original data. In this fashion, 136 coefficients were used to represent the strain data from the vertical section and 176 coefficients from the horizontal section. The larger number of coefficients required to describe the horizontal section would indicate that the strain distribution was more complicated in this region.

The decomposition was performed on both the experimental and simulation data sets, producing a set of coefficients representing each strain field. These coefficients were then plotted against each other for the horizontal and vertical sections, as shown in Fig. 2.8. The experimental coefficients were plotted along the x-axis, and the simulation coefficients along the y-axis. If there were perfect agreement between the two sets of coefficients, the points would all lie along the line with gradient of unity (solid line in the figure).

Deviation from this line indicates differences between the experimental and simulation data sets. In reality, uncertainty in both the experiment and the simulation will cause deviations, and so it is unrealistic to expect all the points to fall on this line. For that reason, Fig. 2.8 has been plotted along with confidence bounds (dashed lines) which relate to the experimental uncertainty. The bands are defined by combining of the uncertainty from the experiment and from the image decomposition reconstruction process. For the case shown here, all of the moments fell within the confidence bounds. The points are primarily concentrated along the solid line, but there are a few moments close to the dashed lines, particularly in the comparison of the vertical section.

2.5 Conclusions

The performance of adhesively bonded structural composite Pi/T-joints was evaluated by experimental pull-out tests and numerical simulations. The values of the peak pull-out force recorded experimentally matched well with those from the numerical simulation (~10 % difference). The vacuum assisted resin transfer molding (VARTM) technique was found to be a successful technique to produce Pi/T-joints. 3-D digital image correlation was used to capture the displacements and strains in the pi-joint during the pull-out tests. The CEN procedure for making quantitative comparisons of measured and predicted

strain fields was applied using image decomposition. The simulation was found to produce acceptable results within the confidence bounds provided by the uncertainty in the experiment. Experimentally validated simulations can be used to further understand the behavior of Pi-joints with other joint configurations and also to understand damage-induced behaviors beyond the case explored in this work, and such validated simulations have great potential in use as a design tool.

Acknowledgements This work was supported by the U.S. Army and ONR under TACOM/MSU Cooperative Agreement No. W56HZV-07-2-0001 and in collaboration with US Army TARDEC. The authors are thankful to Albany Engineered Composites Inc., NH, USA, for supplying the 3D-woven Pi-preforms. EAP was the recipient of a Royal Society Wolfson Research Merit Award.

References

1. Stickler, P.B., Ramulu, M.: Investigation of mechanical behavior of transverse stitched T-joints with PR520 resin in flexure and tension. Compos. Struct. **52**, 307–314 (2001)
2. Flansburg, B.D., Engelstad, S.P.: Robust design of composite bonded Pi joints. 50th AIAA/ASME/ASCE/AHS/ASC Structures, Structural Dynamics, and Materials Conference. Palm Springs, CA (2009)
3. Dulieu-Smith, J.M., Quinn, S., Shenoi, R.A., Read, P.J.C.L., Moy, S.S.J.: Thermoelastic stress analysis of a GRP Tee Joint. Appl. Compos. Mater. **4**, 283–303 (1997)
4. Marcadon, V., Nadot, Y., Roy, A., Gacougnolle, J.L.: Fatigue behavior of T-joints for marine applications. Int. J. Adhes. Adhes. **26**, 481–489 (2006)
5. Li, H.C.H., Dharmawan, F., Herszberg, I., John, S.: Fracture behavior of composite maritime T-joints. Compos. Struct. **75**, 339–350 (2006)
6. Kesavan, A., Deivasigamani, M., John, S., Herszberg, I.: Damage detection in T-joint composite structures. Compos. Struct. **75**, 313–320 (2006)
7. Shenoi, R.A., Violette, F.L.M.: A study of structural composite tee joints in small boats. J. Compos. Mater. **24**, 644–666 (1990)
8. Shenoi, R.A., Hawkins, G.L.: Influence of material and geometry variations on the behaviour of bonded tee connections in FRP ships. Composites **23**, 335–345 (1992)
9. Hicks, I.A., Read, P.J.C.L., Shenoi, R.A.: Tensile compressive and flexural characteristics of tee-joints in foam-cored sandwich structures. Proc. 3rd Int. Conf. Sandwich Construction, 579–590 (1996)
10. Shenoi, R.A., Read, P., Jackson, C.L.: Influence of joint geometry and load regimes on sandwich tee joint behaviour. J. Reinf. Plast. Compos. **17**, 725–740 (1998)
11. Dulieu-Barton, J.M., Earl, J.S., Shenoi, R.A.: Determination of the stress distribution in foam-cored sandwich construction composite tee joints. J. Strain Anal. Eng. Des. **36**, 545–560 (2001)
12. Toftegaard, H., Lystrup, A.: Design and test of lightweight sandwich T-joint for naval ships. Compos. Part A: Appl. Sci. Manuf. **36**, 1055–1065 (2005)
13. Theotokoglou, E.E., Moan, T.: Experimental and numerical study of composite T-joints. J. Compos. Mater. **30**, 190–209 (1996)
14. Theotokoglou, E.E.: Study of the numerical fracture mechanics analysis of compositeT-joints. J. Reinf. Plast. Compos. **18**, 215–223 (1999)
15. Dodkins, A.R., Shenoi, R.A., Hawkins, G.L.: Design of joints and attachments in FRP ships' structures. Mar. Struct. **7**, 365–398 (1994)
16. Theotokoglou, E.E.: Strength of composite T-joints under pull-out loads. J. Reinf. Plast. Compos. **16**, 503–518 (1997)
17. Rispler, A.R., Steven, G.P., Tong, L.: Failure analysis of composite T-joints including inserts. J. Reinf. Plast. Compos. **16**, 1642–1658 (1997)
18. Phillips, H.J., Shenoi, R.A.: Damage tolerance of laminated tee joints in FRP structures. Compos. Part A: Appl. Sci. Manuf. **29**, 465–478 (1998)
19. Banea, M.D., da Silva, L.F.M.: Adhesively bonded joints in composite materials: an overview. J. Mater. Des. Appl. **223**, 1–18 (2009)
20. Haq, M., Patterson, E.A., Drzal, L.T.: Pull-out behavior of adhesively bonded composite Pi-joints: damage modeling and comparison with experiments. Proceedings of the 25th Annual Technical Conference, American Society of Composites, Dayton, OH (2010)
21. Online: Air Force Print News. http://www.wpafb.af.mil/news/story_print.asp?id=123035046 (2009). Accessed 16 Sept 2009
22. Russell, J.D.: Composites affordability initiatives. Adv. Mater. Process. **165**, 29–32 (2007)
23. Haq, M., Conway, A., Patterson, E.A.: A study on damage-induced behavior of bonded Pi-/T-joints using digital image correlation (DIC) and FE modeling, 2012 SEM XII, International Congress and Exposition on Experimental and Applied Mechanics, Costa Mesa, CA (2012)
24. Sebastian, C., Haq, M., Conway, A., Patterson, E.A.: Comparison of FE and DIC measurements of a Pi-joint using feature vectors, 2012 SEM XII, International Congress and Exposition on Experimental and Applied Mechanics, Costa Mesa, CA (2012)
25. Simulia, I.: Abaqus/CAE Version 6.8-2 (2008)
26. CWA16799. Validation of Computational Solid Mechanics Models. Comite European de Normalisation, Brussels (2014)
27. Wang, W., Mottershead, J.E., Ihle, A., Siebert, T., Reinhard Schubach, H.: Finite element model updating from full-field vibration measurement using digital image correlation. J. Sound Vib. **330**(8), 1599–1620 (2011)
28. Sebastian, C.M., Patterson, E.A., Ostberg, D.: Comparison of numerical and experimental strain measurements of a composite protective panel using image decomposition. Appl. Mech. Mater. **70**, 63–68 (2011)
29. Bucinell, R.B.: Composite materials fatigue and fracture, vol. 7. STP-1330 ASTM, PA (1998)
30. Truong, T.C., Vettori, M., Lomov, S., Verpoest, I.: Carbon composites based on multi-axial multi-ply stitched preforms: part 4, mechanical properties and damage observation. Compos. Part A: Appl. Sci. Manuf. **36**, 1207–1221 (2005)

Springer

http://www.springer.com/978-3-319-42425-5

Joining Technologies for Composites and Dissimilar Materials, Volume 10
Proceedings of the 2016 Annual Conference on Experimental and Applied Mechanics
Cloud, G.; Patterson, E.; Backman, D. (Eds.)

2017, VII, 123 p. 111 illus., 91 illus. in color., Hardcover
ISBN: 978-3-319-42425-5